Development of Memory Elements based on Surface-Modified Nanostructured Porous Silicon

TOLAGAY DUISEBAYEV, MARGULAN IBRAIMOV, BAKYT KHANIYEV, AYAN TILEU, DINA ALIMBETOVA
Department of Solid State Physics and Nonlinear Physics,
Al-Farabi Kazakh National University,
71 Al-Farabi Avenue, Almaty,
KAZAKHSTAN

Abstract: - Due to advancements in memory technology, nanostructured semiconductor-based memristors are attracting increasing attention. This article presents the results of a study on memristors based on modified porous structures made from silicon. The memristive properties of nanostructured porous silicon (por-Si) and metal-oxide layers were investigated. The memristors based on por-Si were fabricated using electrochemical etching. The study shows that after 3 minutes, the por-Si film exhibited reversible properties, indicating that memristive behavior was observed in the porous silicon nanofilms. Metal-oxide semiconductor, such as CuO, was deposited on the por-Si surface using magnetron sputtering. The morphology of the por-Si and heterostructure was analyzed using scanning electron microscopy. The influence of light illumination on the memristor properties of films was also observed, with an increase in the hysteresis area dependent on the illumination process.

Key-Words: - memristor, porous silicon, nanofilm, electrical characteristics, hysteresis, magnetron sputtering, memory elements, surface modification.

Received: April 4, 2024. Revised: August 5, 2024. Accepted: September 7, 2023. Published: Ovotber 17, 2024.

1 Introduction

Developing new semiconductor memory types is essential in modern micro- and nanoelectronics applications, [1]. Demand for low-power electronic devices, such as memories, which operate at lower voltages and exhibit ultra-high speed with excellent flexibility, has increased tremendously in this modern era. However, a considerable gap exists between the amount of created data and the available data storage space, which must be satisfied. Hence, there is an urgent requirement for a promising alternative that can effectively replace legacy technology concerning device performance, flexibility, and versatility. Memristor is considered one of the best candidates for the next-generation high-performance nonvolatile memory, logic, and neuromorphic applications, [2], [3], [4], [5]. Memristors are used in many electrical circuits [6], [7], [8], neural networks [9], [10], [11] and neurodynamics [12], [13] due to their simple device structure, reliability, switching endurance, fast reading, and writing. In addition, they are widely applied in nanotechnology industries [14], [15] for their nano-scale device dimensions, low power consumption, and excellent scalability. A similar element was implemented in 2008 by Stanley Williams (Hewlett-Packard) group. It was a thin (30–50 nm) bilayer TiO_2/TiO_2-x film sandwiched between platinum electrodes, [16]. The main characteristic of a memristor, as a passive element of an electrical circuit, is that its resistance is dependent on the integration of the current flowing through it during operation. This means that the element can “remember” the last value of resistance when the power is switched off. The estimated data retention time for this memory is more than 10 years. Several memristor models have been designed, which include the resistive random-access memories [17], TiO_x memristor [18], SiO_x memristor [19], [20], [21], [22], ZnO memristor [23], [24], NiO [25], perovskites [26]. In addition to the experimental studies, considerable attention has been paid to the theoretical modeling of the properties of memristors [27], [28], [29], [30]. Composite materials combining metal oxides along with nanostructured porous materials, especially porous silicon (por-Si), represent a suitable platform for the fabrication of memrisitive elements. Por-Si has a large specific surface area,

fractal nature, and distinctive electrical properties for creating memory cells. The advantage of using por-Si is the simplicity of their production technology and their compatibility with devices of modern silicon microelectronics. In addition, it is possible to control the characteristics of the por-Si by changing the parameters of electrochemical etching. Thus, by depositing metal oxides on the por-Si surface and creating a heterojunction structure, it is possible to improve its memristrive performance at room temperature, [31]. In [32] authors showed the memristive properties and adjustable nature of memristors by embedding NiO into a mesoporous silicon substrate and performing a lateral current scan. Also, [33], reported a memristive device fabrication from nanostructured porous silicon-ZnO/VO_2 composites. [34], designed a bionic double-layer nanoporous structure comprising a Pt/porous $LiCoO_2$/porous SiO_2/Si stack which delivered high memristive performance due to the unique electrochemical properties of porous materials. One of the most attractive semiconductors that can improve the memristive properties of por-Si is CuO due to its electrical and optical properties. Although CuO is one of the most essential semiconductors and can be used in gas sensors, optical devices, electronic materials, batteries etc., there are few reports about its memristive properties. This article discusses the creation of a new nanoscale memristor based on surface-modified nanostructured por-Si nanofilms.

2 Experimental Details

2.1 Porous Silicon Substrate Fabrication

Por-Si layers were obtained by electrochemical etching using p-type boron-doped (100) silicon wafers with a resistivity of 10 Ω·cm and 2 × 10 mm^2 dimensions. The electrochemical etching process was laid out in a special electrochemical cell and was monitored by the power supply. The electrochemical cell is made of highly acidic resistant polymer material such as Teflon. The schematic diagram of the electrochemical etching setup is depicted in Figure 1, [35].

The silicon wafers were dipped into HF (48 %) acid for 5 sec and then cleared with ethanol to remove the unwanted impurities from the surface. The electrolyte solution consists of HF (48 %) acid and ethanol in a volume ratio of 1:1, respectively. The power supply unit has a voltage of 30 V and a current of 5 mA. The etching time was 3 min.

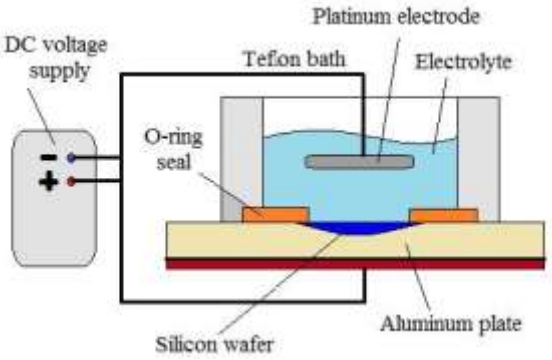

Fig. 1: Electrochemical etching setup

The etched sample porosity was determined by the gravimetric method using the formula (1):

$$p = \frac{m_1 - m_2}{m_1 - m_3} \times 100\%, \qquad (1)$$

where m_1 is the weight of silicon before etching, m_2 is the weight after electrochemical etching, and m_3 is the weight after the removal of porous layer in KOH solution, [35].

2.2 Metal Oxide Layer Deposition

CuO layer was deposited on the surface of the por-Si samples by magnetron sputtering technology. Magnetron sputtering technology advantages are fast deposition speed, deposited films well combined with the substrates, and high purity. The magnetron sputtering process was performed on the Kurt J. Lesker LAB-18 magnetron system (Kurt J. Lesker Company, Dresden, Germany). A CuO target with a purity of 99.999% was used to mount CuO on the por-Si surface, and the distance between the target and the por-Si sample was 13 cm. The base vacuum pressure of the unit was 5· 10-6 Torr, and the working pressure was 10.5 mTorr. In addition, argon (Ar) and oxygen (O_2) gases were introduced into the magnetron sputtering chamber with flow rates of 40 sccm and 10 sccm, respectively. The sputtering power of CuO was 100 W, and the deposition time was 30 min. After depositing CuO on the surface of the por-Si sample, the film was annealed in a special furnace at a temperature of 650°C for 4 hours to obtain a crystalline state.

2.3 Characterization

The morphology and composition of the adsorbents were examined and analyzed by scanning electron microscope (SEM) Quanta 200i 3D using SEM images and EDX spectrum, respectively. Scanning electron microscopy (SEM) images were used to

determine the shape and thickness of the fabricated samples.

The NI ELVIS II+ module was used to measure the current-voltage characteristics of the samples in the voltage range U = 0 – 3 V; the measurement step was 10 mV. The hysteresis behavior in the current-voltage characteristics of the samples was obtained by Keysight B1500A Semiconductor Analyzer. Two ohmic contacts of InGa alloy in the coplanar configuration were deposited on the samples' surface by thermal installation to obtain electrical characteristics as shown in Figure 2.

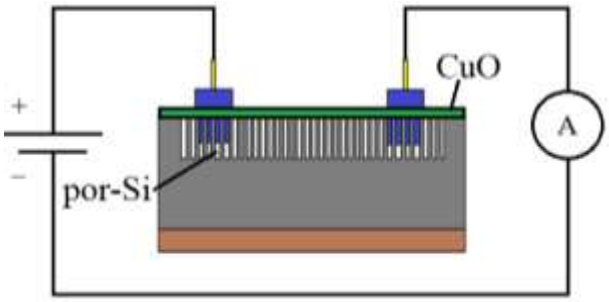

Fig. 2: Configuration of contacts for measurements

3 Results and Discussion

Figure 3 shows cross-sectional and top-view SEM images of the por-Si sample, which was etched for 3 min. Due to electrochemical etching in hydrofluoric acid, the pores were formed with a thickness of 5.16 μm. It can be seen from Figure 2b that pores and air voids are randomly distributed over the entire surface. The porosity value of the por-Si sample was calculated by formula (1) and amounted to 52.6%.

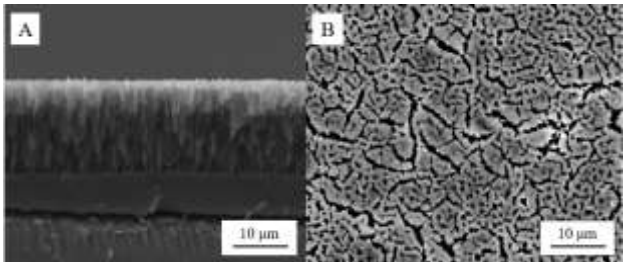

Fig. 3: Cross-sectional (A) and top-view (B) SEM images of the por-Si sample

We performed EDX measurements in conjunction with SEM to analyze the chemical composition of nanostructured material. The result of this study is presented in Figure 4. Silicon is the powder's dominant element.

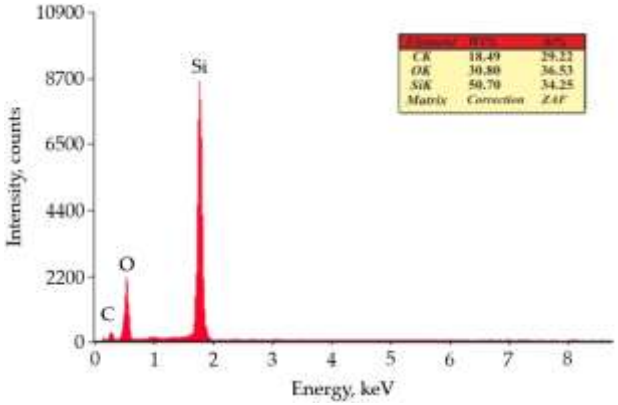

Fig. 4: EDX spectrum of por-Si sample

SEM images of por-Si and CuO/por-Si samples are shown in Figure 5. As can be seen from the figure, the CuO layer which was installed on the surface of the por-Si sample also has a porous structure. Consequently, the pores of the por-Si substrate are not completely closed, which provides a higher surface area and a diffusion channel.

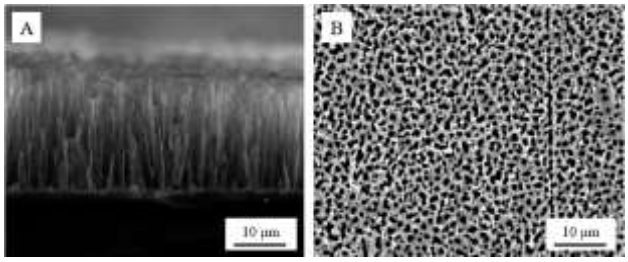

Fig. 5: Cross-sectional (A) and top-view (B) SEM images of the CuO/por-Si samples

Figure 6 shows the current-voltage characteristics of the por-Si sample with measurement intervals of 15 s, 18 s, 1 min, and 3 min, respectively, and shows a positive shift in the current-voltage characteristics after each measurement. It shows that the electrical properties of the por-Si sample depend on the applied voltage and the previous state. After 3 min, the current value of the film returns to its initial state (reset). Accordingly, it is found that the typical memristive behavior of the por-Si sample can be analyzed based on the measurement results. Figure 7 shows the current-time dependence at a voltage of 1.2 V.

At this stage, the phenomenon of hysteresis allows using memristors as memory cells. In some aspects of electronics, they will probably be able to replace semiconductor transistors. The theoretical model described in this work is more straightforward than the modeled theory in published work, [28].

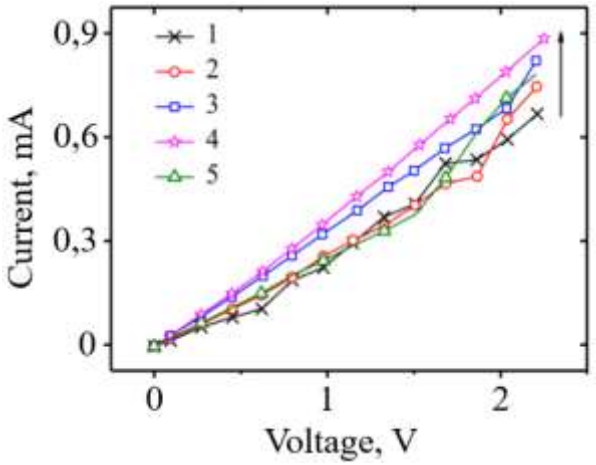

Fig. 6: Current-voltage characteristics at different time intervals, where (1) Initial state, (2) 15 sec, (3) 18 sec, (4) 1 min, (5) 3 min

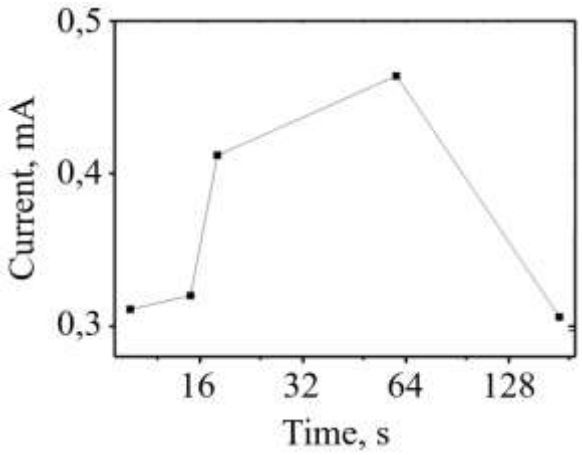

Fig. 7: Current-time dependence at 1.2V

Obtaining nanostructured por-Si films with the properties of a memristor is more accessible than getting structures based on TiO_2 and ZnO. The por-Si memristor does not have the problems of three-terminal memristors [19], such as relatively low switching speed, high power consumption, and lack of a high-density massive structure. In a previous paper [36], the authors of this paper pointed out the presence of hysteresis curves of current-voltage and capacity-voltage characteristics of semiconductor films based on por-Si. The data obtained indicate the memristive properties of the films. So far, we obtained similar physical properties for semiconductor films based on por-Si with the addition of CuO.

The resulting por-Si film also had a hysteresis in the current-voltage characteristics, as in [36]. It was also found that the hysteresis area increased when this film was illuminated by a xenon lamp Oriel Sol3A (I = 0.1 W/cm^2, λVS). Hysteresis in the current-voltage characteristics of the por-Si are shown in Figure 8.

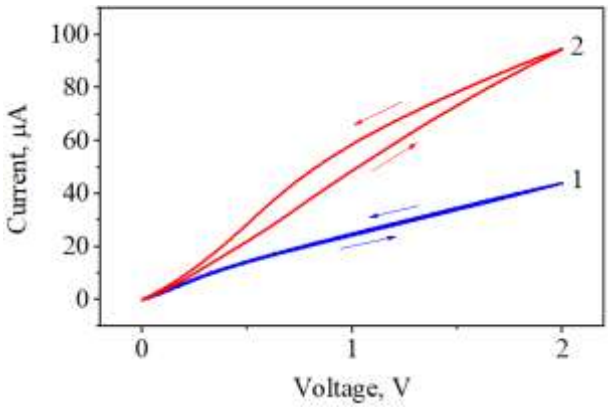

Fig. 8: The current-voltage characteristics of por-Si in the dark (1) and under illumination (2)

CuO/por-Si sample was also exposed to light from a xenon lamp. Exposure to radiation increases the hysteresis area several times, indicating the film's large memristive properties. Graphs and calculations of the hysteresis area in the current-voltage curves are shown in Figure 9:

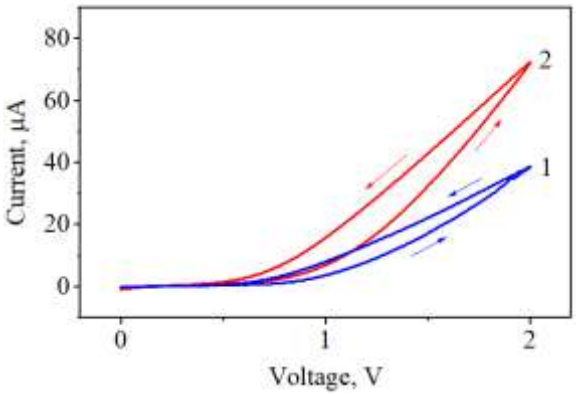

Fig. 9: The current-voltage characteristics of CuO/por-Si in the dark (1) and under illumination (2)

The hysteresis areas were processed and calculated using the Origin package, and their analytical form is presented as follows, [37]:

$$S_H = \frac{1}{2}\left|\begin{matrix} X1 & Y2 \\ Y1 & Y2 \end{matrix}\right| + \left|\begin{matrix} X2 & X3 \\ Y2 & Y3 \end{matrix}\right| + \cdots + \left|\begin{matrix} Xn & Y1 \\ Yn & X1 \end{matrix}\right| \quad (2)$$

As mentioned earlier, the hysteresis curves indicate the presence of memristance properties, and the larger the area, the better these properties manifest. The comparison tables of hysteresis areas depending on illumination are shown in Table 1.

According to data presented in Table 1, the illumination of the films contributes to an increase in the memristor properties. The hysteresis area increases almost 10 times after illumination for the por-Si sample and 2 times for CuO/por-Si.

Table 1 Hysteresis areas dependency on illumination

Hysteresis areas	Samples	
	Por-Si	CuO/por-Si
S1	1.06	5.09
S2	11.2	10.7
S2/S1	10.6	2.1

The properties of films based on por-Si suggest they could be used to create memory cells with optical control. The observed increase in hysteresis when exposed to light is attributed to numerous defects and traps on the por-Si surface, which are crucial for current transfer within the por-Si structure. The nonlinear hysteresis seen in the current-voltage characteristics of these materials is a result of potential barriers within their structure. Additionally, the hysteresis area expands due to the photocurrent generated by incident photons. Photons have enough energy to lift an electron from the valence band to the conduction band. Thus, when light falls on the surface of the samples, their conductivity increases, which leads to an increase in hysteresis. The hysteresis observed in the current-voltage characteristics suggests that resistive switching is mainly driven by the electrochemical migration of oxygen ions through a conduction path within the porous materials, [33]. The deposition and annealing process of CuO leads to the generation of oxygen vacancies. As diffusion constants depend on particle size, with diffusion in bulk being much slower than in nanoparticles due to shortened transport paths, confinement of the metal oxides to a nanoscale size enhances the ionic transport within the porous channels, [38].

4 Conclusion

To conclude, por-Si holds great potential for advancing silicon-based memristive structures, offering a wide array of future applications. The results showed that with appropriate modification, for example by introducing a metal oxide on the surface, improved memristive properties can be achieved. In this work the typical memristive behavior of nanostructured por-Si and metal oxide layer deposited on it was demonstrated and analyzed. Additionally, it was found that obtaining a por-Si nanofilm with memristive properties is simple and does not require additional efforts to develop the device. It was also observed that the hysteresis areas in the current-voltage characteristics of CuO/por-Si significantly increased when exposed to illumination. These characteristics facilitate the development of memory cells and crossbar structures with optical control. Thus, modified nanostructured semiconductors based on por-Si can be essential in successfully implementing practical memristors using economical materials and simple fabrication technologies.

Acknowledgement:
This research is funded by the Ministry of Science and Higher Education of the Republic of Kazakhstan, grant number: AP19678266.

Declaration of Generative AI and AI-assisted Technologies in the Writing Process

During the preparation of this work the authors used Grammarly and DeepL platforms in order to check the grammar of sentences and improve the language of the manuscript. After using this tool/service, the authors reviewed and edited the content as needed and take full responsibility for the content of the publication.

References:

[1] Chua L. Memristor – the missing circuit element, *IEEE Transactions on Circuit Theory,* 1971, 18(5), 507–519. https://doi.org/10.1109/TCT.1971.1083337.

[2] Yang J.J., Pickett M.D., Li X., Ohlberg D.A., Stewart D.R., Williams R.S. Memristive switching mechanism for metal/oxide/metal nanodevices, *Nature Nanotechnology,* 2008, 3, 429-433. https://doi.org/10.1038/nnano.2008.160.

[3] Hu L., Yuan J., Ren Y., Wang Y., Yang J.Q., Zhou Y., Zeng Y.J., Han S.T., Ruan S. Phosphorene/ZnO nano heterojunctions for broadband photonic nonvolatile memory applications, *Advanced Materials,* 2018, 30, 1801232. https://doi.org/10.1002/adma.201801232.

[4] Zhou Y.X., Li Y., Duan N., Wang Z.R., Lu K., Jin M.M., Cheng L., Hu S.Y., Chang T.C., Sun H.J., Xue K.H., Miao X.S. Boolean and Sequential Logic in a One-Memristor-One-Resistor (1M1R) Structure for In-Memory Computing, *Advanced Electronic Materials,* 2018, 4, 1800229, https://doi.org/10.1002/aelm.201800229.

[5] Yan X., Zhang L., Chen H., Li X., Wang J., Liu Q., Lu C., Chen J., Wu H., Zhou P. Graphene oxide quantum dots based memristors with progressive conduction tuning for artificial synaptic learning,

Advanced Functional Materials, 2018, 28, 1803728. https://doi.org/10.1002/adfm.201803728.

[6] Potrebic M., Tosic D. Application of memristors in microwave passive circuits, *Radioengineering,* 2015, 24, 408-419. http://dx.doi.org/10.13164/re.2015.0408.

[7] Amdapurkar A., Naik D.K., Ravi V. Design and Development of Memristor-based Combinational Circuits, *International Journal on Recent and Innovation Trends in Computing and Communication,* 2016, 4, 554–557. https://doi.org/10.17762/ijritcc.v4i3.1937.

[8] Vourkas I., Sirakoulis G.C. Emerging Memristor-Based Logic Circuit Design Approaches: A Review, *IEEE Circuits and Systems Magazine,* 2016, 16, 15–30. https://doi.org/10.1109/MCAS.2016.2583673.

[9] Xu W., Wang J., Yan X. Advances in memristor-based neural networks, *Frontiers in Nanotechnology,* 2021, 3, 645995. https://doi.org/10.3389/fnano.2021.645995.

[10] Yan L., Pei Y., Wang J., He H., Zhao Y., Li X., Wei Y., Yan X. High-speed Si films based threshold switching device and its artificial neuron application, *Applied Physics Letters,* 2021, 119, 153507. https://doi.org/10.1063/5.0063078.

[11] Pan B., Zhang D., Zhang X., Wang H., Bai J., Yang J., Zhang Y., Kang W., Zhao W. Skyrmion Induced Memristive Magnetic Tunnel Junction for Ternary Neural Network, *IEEE Journal of the Electron Devices Society* 2019, 7, 529-533. https://doi.org/10.1109/JEDS.2019.2913637.

[12] Liu N., Yang G., He Y., Ma G., Chen A., Chen Q., Xiong Z., Liu C., Tseng Y.T., Chang T.C., Wang H. Realization of Synapse Behaviors Based on Memristor and Simulation Study with KMCMethod, *IEEE Journal of the Electron Devices Society,* 2020, 8, 981-985. https://doi.org/10.1109/JEDS.2020.3023015.

[13] Cantley K.D., Subramaniam A., Stiegler H.J., Chapman R.A., Vogel E.M. Neural Learning Circuits Utilizing Nano-Crystalline Silicon Transistors and Memristors, *IEEE Transactions on Neural Networks and Learning Systems* 2012, 23, 565-573. https://doi.org/10.1109/tnnls.2012.2184801.

[14] Na S.Y., Yoon S.M. Impacts of HfO2/ZnO Stack-Structured Charge-Trap Layers Controlled by Atomic Layer Deposition on Nonvolatile Memory Characteristics of In-Ga-Zn-O Channel Charge-Trap Memory Thin-Film Transistors, *IEEE Journal of the Electron Devices Society,* 2019,7, 453-461. https://doi.org/10.1109/JEDS.2019.2908255.

[15] Sanchez-Lopez C., Carrasco-Aguilar M.A., Muniz-Montero C. A 16Hz-160kHz memristor emulator circuit, *AEU - International Journal of Electronics and Communications*, 2015, 69, 1208-1219. https://doi.org/10.1016/j.aeue.2015.05.003.

[16] Strukov D.B., Snider G.S., Stewart D.R., Williams R.S. The missing memristor found. *Nature,* 2008, 453, 80-83. https://doi.org/10.1038/nature06932.

[17] Lu B., Lu Y., Zhu H., Zhang J., Yue S., Li S., Zhuge F., Ye Z., Lu J., Memristors based on amorphous ZnSnO films, *Materials Letters,* 2019, 249, 169-172. https://doi.org/10.1016/j.matlet.2019.04.086.

[18] Miller K., Nalwa K.S., Bergerud A., Neihart N.M., Chaudhary S. Memristive Behavior in Thin Anodic Titania, *IEEE Electron Device Letters,* 2010, 31,737-739. https://doi.org/10.1109/LED.2010.2049092.

[19] Choi S., Choi J.W., Kim J.C., Jeong H.Y., Shin J., Jang S., Ham S., Kim N.D., Wang G. Energy-efficient three-terminal SiO_x memristor crossbar array enabled by vertical Si/graphene heterojunction barristor, *Nano Energy,* 2021, 84, 105947. https://doi.org/10.1016/j.nanoen.2021.105947.

[20] Gao Q., Huang A., Hu Q., Zhang X., Chi Y., Li R., Ji Y., Chen X., Zhao R., Wang M., Shi H., Wang M., Cui Y., Xiao Z., Chu P.K. Stability and Repeatability of a Karst-like Hierarchical Porous Silicon Oxide-Based Memristor, *ACS Applied Materials and Interfaces,* 2019, 11, 21734-21740. https://doi.org/10.1021/acsami.9b06855.

[21] Torres-Costa V., Mäkilä E., Granroth S., Kukk E., Salonen J. Synaptic and Fast Switching Memristance in Porous Silicon-Based Structures, *Nanomaterials,* 2019, 9, 825. https://doi.org/10.3390/nano9060825.

[22] Nandakumar S.R., Minvielle M., Nagar S., Dubourdieu C., Rajendran B. A 250 mV $Cu/SiO_2/W$ Memristor with Half-Integer Quantum Conductance States, *Nano Letters,* 2016, 16, 1602-1608. https://doi.org/10.1021/acs.nanolett.5b04296.

[23] Martinez L., Ocampo O., Kumar Y., Agarwal V. ZnO-porous silicon nanocomposite for possible memristive device fabrication, *Nanoscale Research Letters,* 2014, 9, 1-6. https://doi.org/10.1186/1556-276x-9-437.

[24] Park J., Lee S., Lee J., Yong K. A light incident angle switchable ZnO nanorod memristor reversible switching behavior between two non-volatile memory devices, *Advanced Materials,* 2013, 25, 6423-6429. https://doi.org/10.1002/adma.201303017.

[25] Zhu Y.B., Zheng K., Wu X., Ang, L.K. Enhanced stability of filament-type resistive switching by interface engineering, *Scientific reports,* 2017, 7(1), 43664. https://doi.org/10.1038/srep43664.

[26] Sawa A., Fujii T., Kawasaki M., Tokura Y. Hysteretic current-voltage characteristics and resistance switching at a rectifying Ti/$Pr_{0.7}Ca_{0.3}MnO_3$ interface, *Applied Physics Letters,* 2004, 85(18), 4073-4075. https://doi.org/10.1063/1.1812580.

[27] Amarnath N., Ramakrishnan V.N. Modeling and Simulation of Gated Memristor, *Materials Today: Proceedings*, 2020, 24, 1777–1787. https://doi.org/10.1016/j.matpr.2020.03.602.

[28] Hacer A.Y. New area efficient memristor realizations, *Microelectronics Journal,* 2021, 111, 105037. https://doi.org/10.1016/j.mejo.2021.105037.

[29] Ibrahim M.A., Minaei S., Kuntman H. A 22.5MHz current-mode KHN-biquad using differential voltage current conveyor and grounded passive elements, *AEU – International Journal of Electronics and Communications,* 2005, 59, 311-318. https://doi.org/10.1016/j.aeue.2004.11.027.

[30] Pershin Y.V., Ventra M.D. Memory effects in complex materials and nanoscale systems, *Advances in Physics,* 2011, 60, 145-227. https://doi.org/10.1080/00018732.2010.544961.

[31] Khaniyev B.A., Ibraimov M.K., Sagidolda Y., Tezekbay Y., Duisebayev T.S., Tileu A.O., Khaniyeva A.K. The Improved Non-Polar Gas sensing performance of Surface-Modified Porous silicon-based gas sensors, *Coatings,* 2023, 13, 190. https://doi.org/10.3390/coatings13010190.

[32] Mares J. W., Fain J. S., Weiss S. M. Variable conductivity of nanocomposite nickel oxide/porous silicon, *Physical Review B – Condensed Matter and Materials Physics,* 2013, 88(7), 075307. https://doi.org/10.1103/PhysRevB.88.075307.

[33] Ocampo O., Antunez E.E., Agarwal V. Memristive devices from porous silicon – ZnO/VO_2 nanocomposites, *Superlattices and Microstructures,* 2015, 88, 198-203. https://doi.org/10.1016/j.spmi.2015.09.012.

[34] Gao Q., Huang A., Zhang J., Ji Y., Zhang J., Chen X., Geng X., Hu G., Wang M., Xiao Z., Chu P.K. Artificial synapses with a sponge-like double-layer porous oxide memristor, *NPG Asia Materials*, 2021, 13(1), 3. https://doi.org/10.1038/s41427-020-00274-9.

[35] Khaniyev B.A., Sagidolda Y., Dikhanbayev K.K., Tileu A.O., Ibraimov M.K. High sensitive NH3 sensor based on electrochemically etched porous silicon, *Cogent Engineering,* 2020, 1810880. https://doi.org/10.1080/23311916.2020.1810880.

[36] Zhanabaev Z.Z., Turlykozhayeva D., Ikramova S., Tileu A., Maksutova A., Khaniyev B., Khaniyeva A. Current and capacitance hysteresis in porous semiconductor nanofilms. *Physical Sciences and Technology*, 2020, 7, 36-42. https://doi.org/10.26577/phst.2020.v7.i2.06.

[37] Origin Labs – Polygon Area, [Online]. https://www.originlab.com/doc/origin-help/math-polygonarea (Accessed Date: September 10, 2024).

[38] Malik R., Burch D., Bazant M., Ceder G. Particle size dependence of the ionic diffusivity *Nano letters,* 2010, 10, 4123-4127. https://doi.org/10.1021/nl1023595.

Contribution of Individual Authors to the Creation of a Scientific Article (Ghostwriting Policy)

The authors equally contributed to the present research, at all stages from the formulation of the problem to the final findings and solution.

Sources of Funding for Research Presented in a Scientific Article or Scientific Article Itself

This research is funded by the Ministry of Science and Higher Education of the Republic of Kazakhstan, grant number: AP19678266.

Conflict of Interest

The authors have no conflicts of interest to declare.